Proceedings of 20th International Congress on Acoustics, ICA 2010

23-27 August 2010, Sydney, Australia

Enhancement of acoustic heating during nucleation of acoustic cavitation inside an ultrasonic reactor cavity

Marc Hauptmann[1,2], Steven Brems[1], Elisabeth Camerotto[1,3], XiuMei Xu[1], Herbert Struyf[1], Paul Mertens[1], Marc Heyns[1,4], Stefan De Gendt[1,3], Christ Glorieux[2] and Walter Lauriks[2]

(1) IMEC vzw, Leuven, Belgium
(2) Laboratorium voor Akoestiek en Thermische Fysica, Katholieke Universiteit Leuven, Belgium
(3) Afdeling Moleculair Design en Synthese, Katholieke Universiteit Leuven, Belgium
(4) Departement Metaalkunde en Toegepaste Materiaalkunde, Katholieke Universiteit Leuven, Belgium

PACS: 43.25.Yw , 43.35.Ei, 43.35.Hl, 43.35.Sx

ABSTRACT

In semiconductor manufacturing, megasonic cleaning may play an important role for nano-particle removal, if the underlying physical processes are thoroughly understood. As shown in recent years, acoustic cavitation is the main contributor to surface cleaning. Crucial parts of the overall cleaning process are therefore the actual nucleation of cavitation bubbles in the bulk of the liquid and related physical processes that might enhance, suppress or simply accompany bubble nucleation. One process is the enhanced build-up of temperature gradients in ultrasonic fields due to nucleation onset and the accompanied collapse of the nucleating bubbles. There, the highly non-linear oscillatory behaviour of resonant cavitation bubbles might enhance dissipation of acoustic energy and heat transfer from the vicinity of the collapsing bubble to the surrounding liquid. The resulting convection and its relation to the nonlinear interactions of the cavitation bubbles with the acoustic field are investigated in the present study with the help of qualitative and quantitative methods such as Schlieren-imaging and Sonoluminescence Measurements. These methods provide the advantage, that they do not disturb the nucleation process and are applicable to measurements of both pressure and temperature gradients. In order to identify the contribution of the strongly nonlinear bubble-wall oscillations to the enhanced heating of the bulk liquid, the results are correlated to acoustic noise spectra recorded in parallel with the help of a hydrophone.

INTRODUCTION

An important problem in semiconductor surface cleaning is the removal of micro- and nano-sized particulate residues resulting from fabrication steps such as etch and chemical-mechanical polishing. Physical cleaning methods like megasonic cleaning are promising candidates for addressing this issue while minimizing chemical attack of the wafer surface. Here, acoustic cavitation has been identified as both the main cleaning agent as well as the source of structural damage at the wafer surface [1, 2, 3]. The transition between cleaning and damaging behaviour is thereby strongly depending on the stability of the oscillating gas bubbles and their size distribution, which is a consequence of the complex interplay between bubble nucleation, rectified diffusion and bubble collapse [4]. Bubble growth via rectified diffusion is limited to bubbles, which show significant oscillatory activity and are either driven near their (linear) resonance frequency or at one of their sub harmonics, when the pressure amplitude is sufficiently high [5]. At driving frequencies in the MHz-region, the growing bubbles will either immediately reach the threshold for bubble collapse or reach a stable equilibrium size [6]. As a consequence of transient collapse in the first and shape instabilities in the later case, bubble fragmentation will finally lead to a continuous reinitiation of the rectified diffusion process in a self-supported fashion.

To minimize damage and obtain a better control over the bubble-size distribution, working at lower pressure amplitudes and gasification levels is desired. As a consequence, the onset of acoustic cavition in the initial stage might show a delay with respect to the start of the application of the acoustic field. During this stage, the pre-condensed bubble nuclei might show significant activity resulting in acoustic emission at sub- and higher harmonics [6], acoustically induced heating [7,8] and multibubble sonoluminescence [9] (when reaching the bubble collapse threshold). For a fundamental study of the nucleation process, correlation of those experimental parameters might give insight in the underlying physical processes [10,11].

In the present work, the nucleation process of bubbles is studied in gasified, ultrapure water (UPW). Thereby, a temporal correlation of acoustic emission at the sub and higher harmonics with time-resolved temperature measurements yields information on the presence and transformation of stable oscillating bubble nuclei during the sonification process. The simultaneous recording of sonoluminescence (SL) activity reveals information on the occurrence of unstable (transient) cavitation. This is suspected to “spark” the regime of acoustic cavitation with continuous reinitiation of the growth- and collapse-cycle of resonant bubbles. High-speed stroboscopic Schlieren imaging of the final nucleation onset is utilized to visualize the interaction of the nucleating bubbles with the

soundfield and the thermal convection resulting from excessive acoustic dissipation at this stage.

THEORY

Rectified Diffusion

Inactive bubbles are subject to surface tension and will therefore dissolve in a liquid (even if it is saturated) unless they are stabilized through organic contamination at the air-liquid interface or the presence of a solid boundary [4]. In contrary, rectified diffusion is a process, where oscillating bubbles in a gasified liquid will experience a net-influx of gas during one cavitation cycle for 2 reasons:

- The difference of bubble surface area between stages of compressions and expansion
- The difference of thickness of the diffusion boundary layer adjacent to the bubble wall between these two stages

The net mass flux will therefore be strongly determined by the driving frequency f_0, the driving pressure amplitude P_a, the bubble equilibrium radius R_n and the relative gas concentration χ_c. Combining Fick's law for mass transfer and the equations of motion for the bubble wall yields an expression for the rectified diffusion threshold (RDT) [12]:

$$\chi_c = \left[1 + \frac{2\sigma}{R_n P_0}\right]\frac{A}{B} \qquad (1)$$

Here, σ denotes the surface tension at the gas-liquid interface, P_0 the ambient pressure, A the time average of the oscillatory bubble radius R normalized by R_n, R/R_n, and B the time average of $(R/R_n)^4$. The value of P_a for which (1) is fulfilled corresponds to the driving pressure amplitude for which a bubble is at equilibrium, meaning that it will neither grow nor shrink.

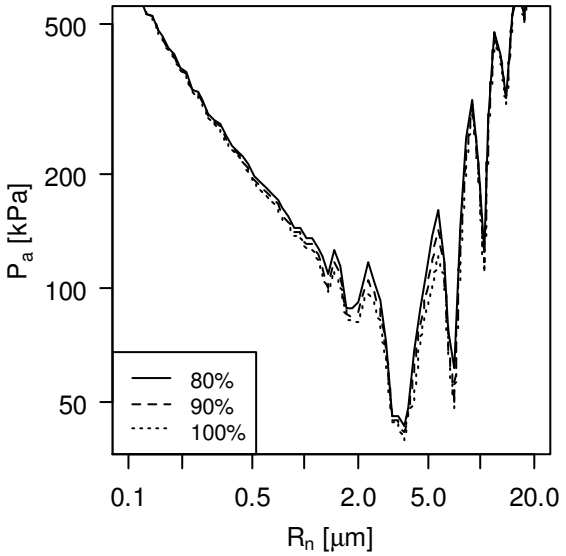

Figure 1. RDT at 0.835 MHz for Argon at relative gas concentrations of 80, 90 and 100% of saturation (61 ppm).

We calculated the RDT for different concentrations of argon using a method similar to that in [13]. As an appropriate model for the underlying bubble dynamics we choose the Keller-Miksis-Model as it is numerically uncomplicated and provides corrections for viscous, thermal and radiation damping as well as for first order in liquid compressibility [14]. If combined with Properetti's correction for the polytropic coefficient [15] in terms of an instantaneous Peclet number [16], the yielded results will be valid over a wide range of driving pressure amplitudes.

Figure 1 shows the RDT for Argon being calculated for gas concentrations of 80%, 90% and 100% of the saturation level (61 ppm or mg/l). Each line represents a boundary in the parameter space spanned by the bubble equilibrium radius and the pressure amplitude of the sound field, above which bubbles will grow due to rectified diffusion and below which they will dissolve. While the RDT displays a monotonical decrease with the gas concentration for all R_n, the dependency on the bubble size itself is rather non-monotonical. Generally, the RDT decreases with bubble sizes approaching the linear resonance until reaching a minimum at the resonance radius itself. Especially in the regime of bubbles larger than resonance size, additional local minima of the RDT can be observed, where one of the oscillating bubbles' higher harmonics meets the frequency of the sound field. A similar behaviour can be observed around a bubble size of 2 µm, this time corresponding to driving at a subharmonic resonance. The appearance of both sub- and higher harmonic resonances is a characteristic feature to non-linear oscillators such as bubbles [17]. A bubble with an initial radius corresponding to the descending branch of the RDT will therefore grow towards the resonance radius with increasing growth rate. If there were no transient collapses, the bubble would grow further until its path in the phase-diagram intersects with the RDT again. The differences in the RDT for different gasification levels are less significant than experiments with varying levels of gasification would suggest. However, the sizes of the initial "seed" bubbles might vary considerably with the gas content of the liquid.

Bifurcation, stable and transient cavitation

Bubbles driven with sufficient pressure amplitudes will act as active scatterers of the sound field. The ratio of acoustic energy scattered by the bubble and the intensity of the sound field is commonly referred to as the acoustic scattering crosssection [4]:

$$\Omega_{mean} = 8\pi \frac{< q(t)^2 >}{P_a^{\,2}} \qquad (2)$$

Eq. (2) has been reformulated for sinusoidal driving with $<P_a^{\,2}>=½$, where <> denotes a time-average. $q(t)$ represents the wavefront amplitude of the spherical wave emitted by a pulsating bubble and incorporates -besides the radial bubble oscillation $R(t)$ - the oscillatory velocity and acceleration of the bubble wall (represented by the time-derivatives of $R(t)$)[18,19]:

$$q(t) = \rho_l R(t) \cdot \left[2\dot{R}(t)^2 + R(t)\ddot{R}(t)\right] \qquad (3)$$

The meaning of Ω can be better understood if compared to the geometrical scattering crosssection Ω_{geom}. This is given by the area, which would be "blocked" by an inactive bubble if it was situated in a unidirectional soundfield. This bubble would leave an acoustic shadow behind, whose crosssection area is given by $\pi R_n^{\,2}$. Oscillating bubbles scatter the acoustic field also actively, leading to an effectively larger portion of the sound field scattered than described by $\Omega_{geom}=\pi R_n^{\,2}$ alone. Thus, a fraction of $\Omega_{mean}/\Omega_{geom} >>1$ will mark the transition from passive to active scattering. Due to the nonlinear nature of the underlying radial oscillations, the spectrum of Ω does generally not only contain the driving frequency. Components at multiples and fractions of f_0 are very likely to be found depending on the size and state of the oscillating bub-

ble. A Fourier analysis of Ω gives information on the expected signal-strengths at the respective frequencies. For instance, bubbles around the linear resonance size (there where the global minimum of the RDT is to be found) will start to show nonlinear behaviour at values of

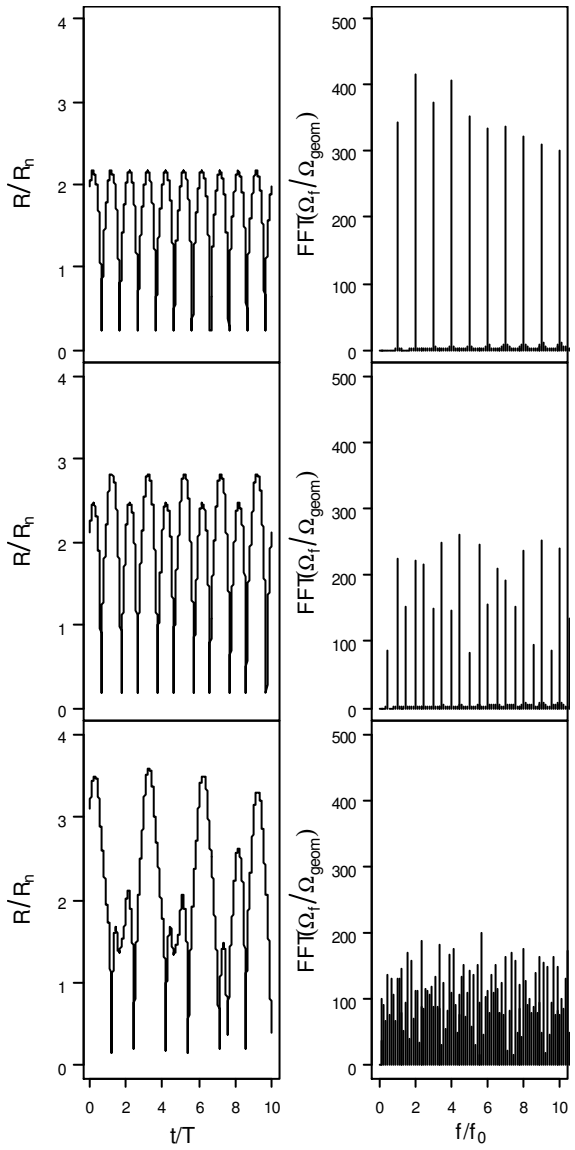

Figure 2. Comparison of the oscillatory response of a bubble with R_n=3.5 µm for different pressure amplitudes. The right graphs show the corresponding emission spectra normalized to the driving frequency f_0.

P_a around athmospheric pressure (100 kPa, Fig. 2) with a maximum of their emission at twice the driving frequency f_0 of the soundfield. This component is usually termed the second harmonic. If the pressure amplitude is further increased, they bubbles will show a secondary effect termed bifurcation (250kPa, Fig. 3) [20]. Their oscillations will remain periodic, but with a main frequency corresponding to half the driving frequency. As a consequence, the secondary sound field emitted by those bubbles will contain additional spectral components at 0.5, 1.5, 2.5, etc. times the driving frequency, where the 0.5-component is usually termed the first subharmonic.

This is accompanied by a general decrease of the signal strengthes of the individual components, as more spectral components appear. With increasing P_a bifurcation will advance and subsequently more subharmonics (and non-integer higher harmonics) will appear in the spectrum. At sufficiently high P_a the oscillations will become fully non-periodic (transient, see Fig. 3 at 300 kPa) with the bubble emission spectra being broad and non-discrete. However, in practice, bubbles at these frequencies are likely to reach the transient state without surpassing bifurcation, as they are likely to become unstable and disintegrate if the maximum bubble radius during one oscillation is becoming larger than approximately 2.3 times the equilibrium radius [21].

We therefore plotted different transient cavitation thresholds (TCT) defined as R/R_n=2.3, 3 and 5 together with the RDT. For the R/R_n=2.3 criterium, the TCT-curve will generally follow the RDT-curve closely.

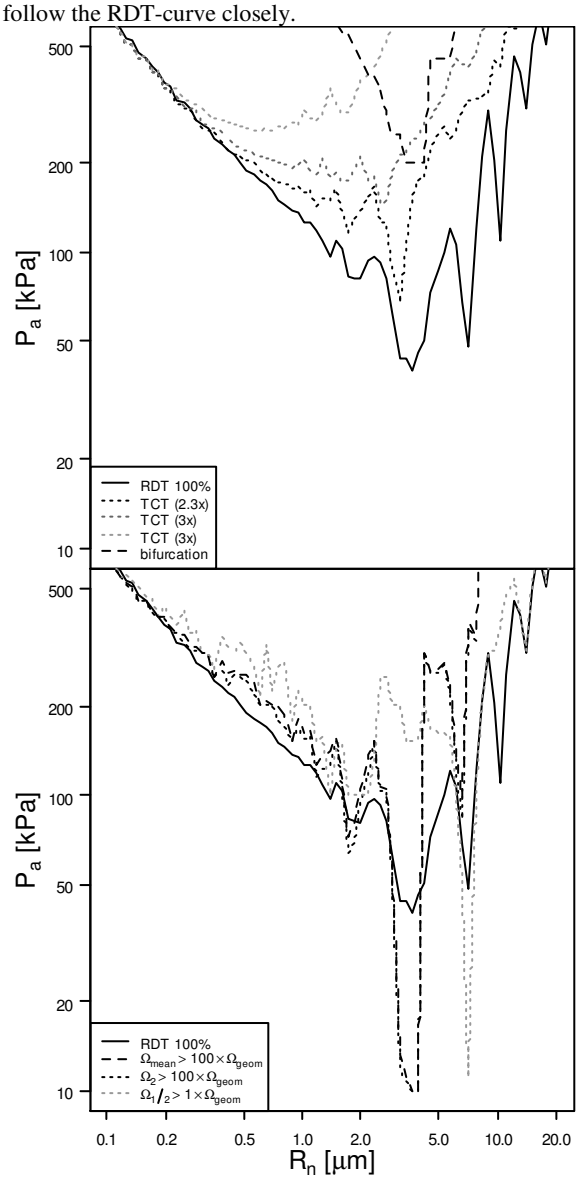

Figure 3. Rectified diffusion, bifurcation, transient cavitation and acoustic scattering thresholds for argon bubbles driven at 0.835 MHz.

Bubbles will therefore become either immediately transient, trapped at one point of the RDT curve or simply dissolve away. According to [13] the fraction of bubbles actually growing to reach the TCT and collapse is only 20%.

If the R/R_n=3 and 5 criteria applied, resonant bubbles would be able to reach the threshold for the onset of bifurcation, but as this lies at rather high pressures, the described process would be rather unrealistic. In order to find regions of increased acoustic activity and identify additional sources for second harmonic and first subharmonic emission, we took the first subharmonic and second harmonic components $\Omega_{½}$ and Ω_2 of the acoustic scattering crossection defined by (2). We then defined acoustic scattering thresholds by normalizing

these scattering crosssections to the geometrical crosssection $\Omega_{geom}=\pi R_n^2$. As a threshold for acoustic scattering, we defined the value of P_a where Ω_2/Ω_{geom} and $\Omega_{mean}/\Omega_{geom}=100$. As the subharmonic emission is expected to be much weaker than the integer higher harmonics or the average signal itself, we used a threshold defined over $\Omega_{½}/\Omega_{geom}=1$ for defining the acoustic scattering threshold there. It is clearly visible, that emission at the second harmonic is mainly characteristic for resonant bubbles. The curve coincides with the threshold for Ω_{mean}, which indicates enhanced overall acoustic activity for bubbles in that size range, giving rise to secondary effects such as acoustic heating. Subharmonic emission is obviously limited to bubbles with twice the resonance size. Those bubbles will be driven at their first higher harmonic, leading to an oscillation mainly at their own resonance frequency and subharmonic emission even at low driving pressures (Fig. 4, [22]).

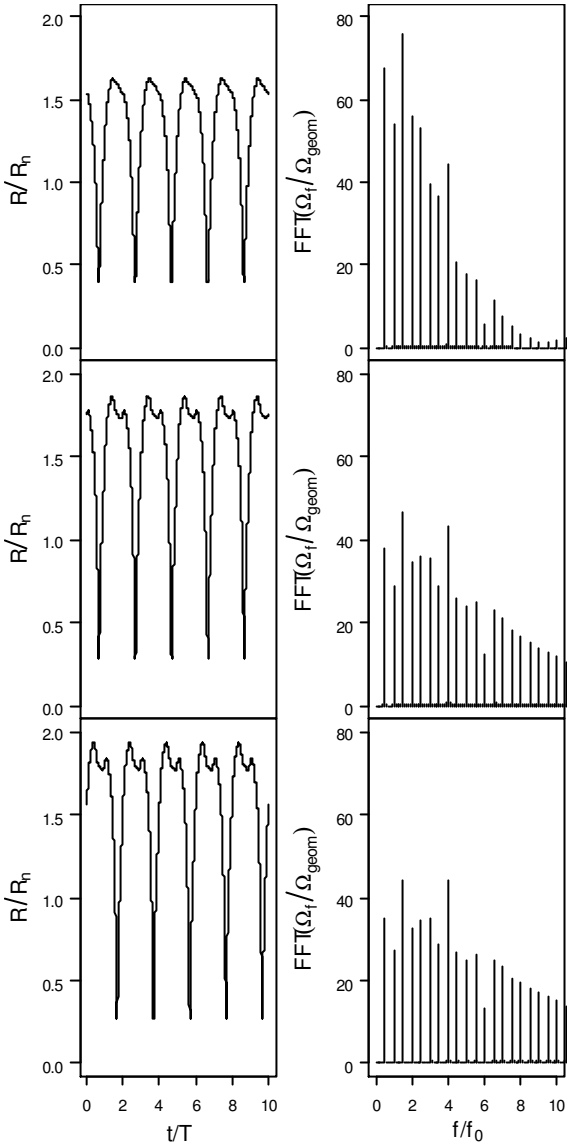

Figure 4. Comparison of the oscillatory response of a bubble with R_n=7 µm for different pressure amplitudes. The right graphs feature the corresponding emission spectra normalized to the driving frequency f_0.

As stated above, the growth of bubbles to larger radii via rectified diffusion might be an unrealistic scenario. However, shape instabilities might enhance rectified diffusion through microstreaming and produce larger bubbles than predicted. Those bubbles, which are showing oscillations of their surface, are likely subject to the emission of microbubbles. These might have radii close to resonance size and will initially lie above the TCT [23]. The shape instable bubbles might produce subharmonics as well, but due to the dipole nature of their acoustic emission only bubbles very close or attached to the hydrophone might produce significant signals [24].

Boundary Layer Effects and Heating

Acoustic dissipation is known to influence temperature measurements with thermo sensors or -couples, which may display an increase in temperature limited to the duration of sonication. This is strongly depending on geometric and material properties of the utilized thermal probes such as surface area, thermal resistance and conversion efficiency. Thus, the informative value of absolute temperature measurements in sonicated liquids might be questionable. Nevertheless, relative (differential) temperature measurements might pose a chance to gather additional information on the acoustic activity of bubbles present in the MHz-sound field [10]. The dissipation of acoustic energy near a solid-liquid boundary such as the wall of the reactor vessel or the surface of a thermometer usually exceeds simple bulk dissipation at those spots. The reason is the formation of an acoustic boundary layer which exhibits large gradients of the oscillatory particle velocity that counteract the mechanical coupling of the fluid particles [25]. To get an idea of the response of a thermocouple with specific properties, we modify Laplace law of thermal conduction [26] to include a source term for the power dP_{diss}/dA dissipated per surface area in the boundary layer with thickness δ and a "specific" surface A^* of the thermo element including its somewhat intrinsic properties. We now obtain an ordinary linear differential equation that can be solved analytically:

$$\frac{1}{C_v}\frac{dP_{diss}}{\delta dA}=\frac{dT}{dt}+\frac{\kappa}{A^*}(T-T_0)$$
$$T(t)=\frac{1}{C_v}\frac{dP_{diss}}{\delta dA}\frac{A^*}{\kappa}\left[1-\exp\left(-\frac{\kappa}{A*}t\right)\right]+T_0 \quad (3)$$

C_v and κ are the volumetric heat capacitance at constant volume and the thermal diffusivity of water, respectively. With κ=0.142mm^2/s [26] and A*=1mm^2 one gets a time constant of around 7s, which is in the same order of magnitude as observed in the experiment. The term containing dP_{diss}/dA in the solution for the time dependency of $T(t)$ will give the saturation value of the increase in temperature measured during sonication. Assuming, acoustic dissipation at the walls of an ultrasonic vessel is limited to 0.1mW/cm^2 (typical power densities in the ultrasonic field will be in the order of magnitude of W/cm^2), then with d=0.5µm [25, for 1MHz] and C_v=4.2 J/lK this value will be in the range of 3 to 4 °C, which is again observable in experiments. As acoustic dissipation increases with frequency, the presence of higher harmonics in the sound field might give rise to a further enhancement of measured "sonication" temperature. Furthermore, actual heating of the bulk liquid might cause a difference between the liquid temperature before and after sonication.

From medical ultrasound, it is known that microbubbles can enhance acoustic heating both locally [19] as well as globally [27]. The main mechanisms thereby are the emission of high frequency ultrasound due to strongly non-linear pulsation of the acoustically driven bubbles and the subsequent absorption of this high frequency ultrasound by the surrounding liquid. Liquid temperatures in the very vicinity of those bubbles might temporally exceed bulk values by 100K and

more [28], while the bulk of the liquid might heat up with rates of °C/min [29] under continuous irradiation.

EXPERIMENT

Experimental Setup

The setup used in these experiments consists of a water cooled transducer with a resonance frequency of 835kHz on which a small Pyrex beaker is glued. In order to eliminate reflections of the acoustic waves and thus promote the generation of a purely propagating wave, a slice of damping material is located at the endface of the cylindrical beaker. The system is driven with a combination of a function generator and an amplifier (National Instruments PCI-5401 and HAS4101, NF). During megasonic operation, the SL signal is detected with a photomultiplier tube (Hamamatsu R960). In order to improve the sensitivity, a concave mirror is placed at the backside of the cell, while the photomultiplier is located at the front side at the mirror's focal point. The acoustic pressure is measured with a needle hydrophon (Ondacorp HNR-500) with its tip placed ca. 1cm apart from the surface of the damping material. Both the Photomultiplier and the hydrophon signal are recorded with an oscilloscope card (National Instruments PCI-5102), which is synchronized with the function generator and records waveforms with a repetition rate of approximately $1s^{-1}$. The temperature is measured with a T-type thermocouple placed near the lower inlet of the beaker approximately 2cm apart from the bottom plate. The signal is tracked at a repetition rate of 1/s with a multimeter (Fluke 53-II) whose timestamp is synchronized to the control-PC's internal clock. The measurements are automated with LabView, excluding the temperature measurement, which has to be started manually. In this way, all 3 signals can be correlated to each other with respect to the onset of sonification.

To minimize electrical interference and background signal, the system is placed in a Faraday cage, sealed from external light. The liquid flow can be regulated between 0 and 1.5 l/min and the gas content of the liquid is controlled with a gasification system described elsewhere [30]. The degassed and purified water is gasified with Argon, since it is known that noble gases significantly amplify the SL signal due to their higher polytropic coefficient [31]. The Ar content is determined from oxygen calibration data.

While measuring SL, temperature and sound pressure, the liquid circulation is set off. In this way, the boundary layer heating described previously is not corrupted by forced convection and overall heating of the bulk liquid can be registered after the acoustic field has been set off. Prior to filling the cell with gasified water, the interior is purged with degassed water under sonication at an acoustic power density of $3W/cm^2$. By this, bubbles from previous experimental cycles which could initialize unwanted transient cavitation are removed from the cell as they dissolve or being dragged away by the flow. Next, the cell is filled at a flow rate of 1.4l/min in order to guarantee a stable gasification level.

Experimental Results

Figure 5 shows the time development of the measured change in temperature *dT* after the onset of the acoustic field. The acoustic power density is set to $3W/cm^2$. All graphs clearly show the exponential onset with start of the sonication. For low gasification levels (89% of the saturation level), *dT* remains rather stable over the whole processing time of 2min. After turning off the acoustic field, *dT* relaxes exponentially as expected, settling at a level of 1K. This temperature difference represents the bulk heating, caused solely by the dissipation of the acoustic energy through both bulk and boundary layer absorption in the liquid and in the damping material. With increasing gasification (94, 97, 100% of the saturation level), the initial plateau reached after sonication onset is followed by a stage of enhanced heating after approximately half of the sonication time (1 min). Both the slope and the peak value increase with gasification level, while almost no increase in the bulk liquid temperature could be registered after the acoustic field has been turned off. This indicates that the observed effect is actually of secondary nature, caused by the active scattering of the sound field by the bubbles and the accompanied appearance of higher frequencies in the sound spectrum. Once the saturation level is surpassed, an overall change in the time dependency of *dT* is evident. The time development of *dT* shows a general enhancement over the whole duration of the experiment compared to *dT* at lower gasification levels. This change is attributed to the onset of cavitation nucleation, where large bubbles appear in the sound field. This is accompanied by dramatic attenuation of the sound field, leading to a sudden relaxation of *dT* during the onset. With increasing gasification level, the nucleation onset occurs after shorter duration of sonication. The nucleation also seems to have an influence on the bulk heating of the liquid which is visible both when the acoustic power is immediately shut off after onset (100%) or kept running (102%).

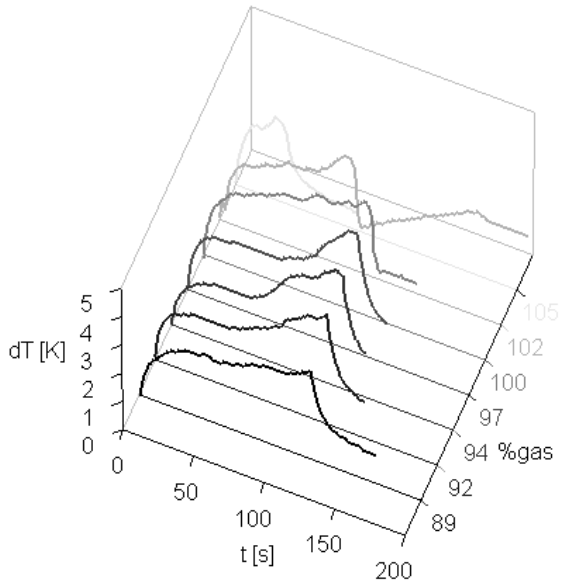

Figure 5. Differential temperature –time curves for Argon at various gasification levels.

A correlation of the temperature data with the respective acoustic emission spectra and SL measurements yields new information on the activity of bubbles at different levels of gasification. Therefore, we plotted the measured PMT signal together with *dT* and the normalized spectral pressure field components in Figures 6 a-d. Next to the amplitude signal, which contains overall information over stability and/or attenuation of the sound field, we plotted the first subharmonic, second harmonic and the sum of all higher harmonic components after normalizing them to the amplitude value. To account for the different signal levels at the respective frequencies, we multiplied the obtained values by 500, 10 and 20 respectively prior to drawing.

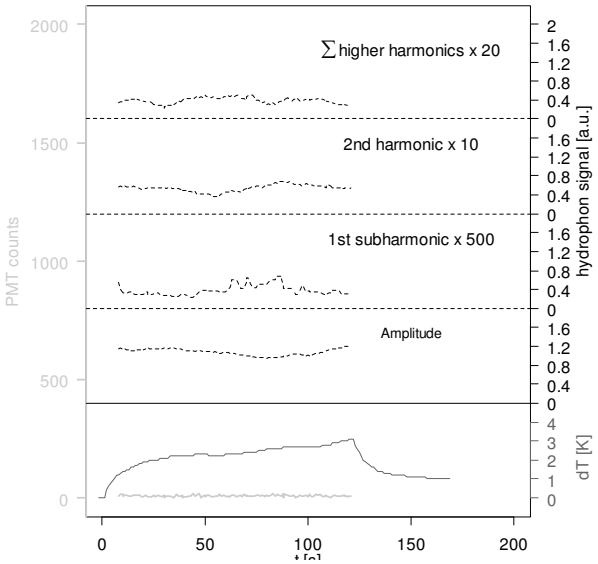

Figure 6 a. Photomultiplier signal, differential temperatur measurement and sound spectrum for Argon at 89% gasification and a power density of 3 W/cm^2.

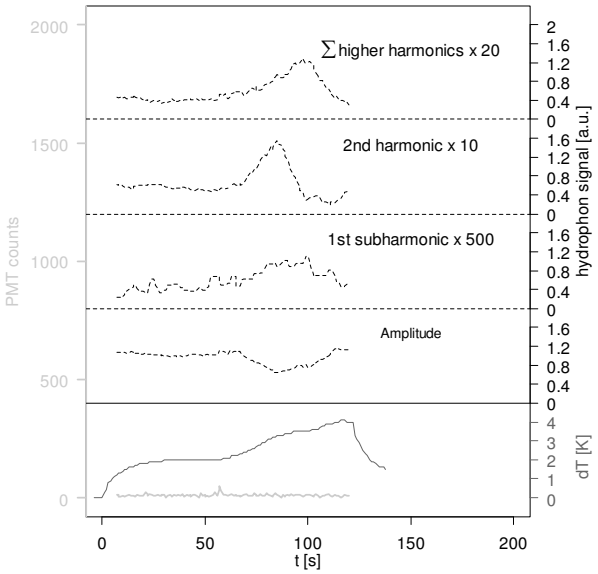

Figure 6 b. Photomultiplier signal, differential temperatur measurement and sound spectrum for Argon at 94% gasification and a power density of 3 W/cm^2.

We observed the most significant differences in all 3 observables between gassification levels of 89% and 94% (Figure 6 a and b). While the signal profiles of temperature, SL and acoustic emission at 89% remain flat during the whole duration of sonification, a stage of enhanced acoustic and thermal activity is preceded by a short burst of sonoluminescent light emission in case of 94% gas content. This initial sonoluminescent signal is then followed by decrease in overall pressure amplitude, as well as a steep increase of the second harmonic signal. A slower response of both the first sub- and overall higher harmonics signals can be seen as well. The data suggest the onset of nucleation initialized by transient cavitation, which is localized to certain areas as the vicinity of the (resonant) bottom plate of the beaker or the surface of the damping material. The localization of the nucleated bubbles weakens the acoustic field due to absorption and incoherent reflection, thus lowering the effective P_a-value below the TCT, but still leaving it above the RDT. As the bubbles are now growing towards twice the resonance size, both the overall higher and subharmonic emission is enhanced. This is accompanied by increased boundary layer heating until the bubbles have presumbly grown out of this resonant region again.

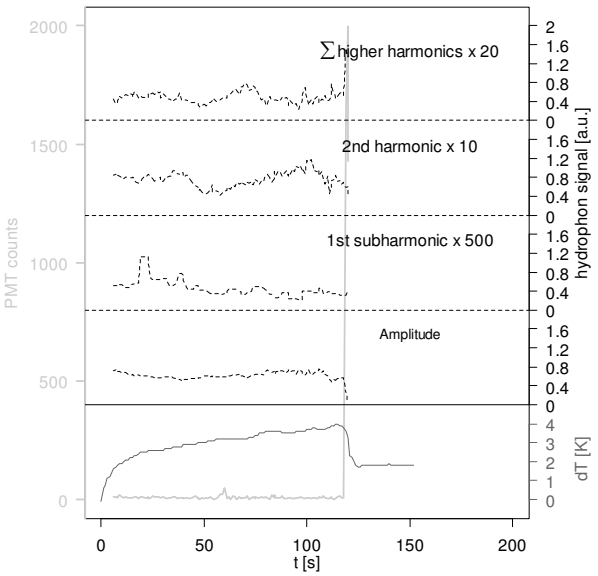

Figure 6 c. Photomultiplier signal, differential temperatur measurement and sound spectrum for Argon at 100% gasification and a power density of 3 W/cm^2.

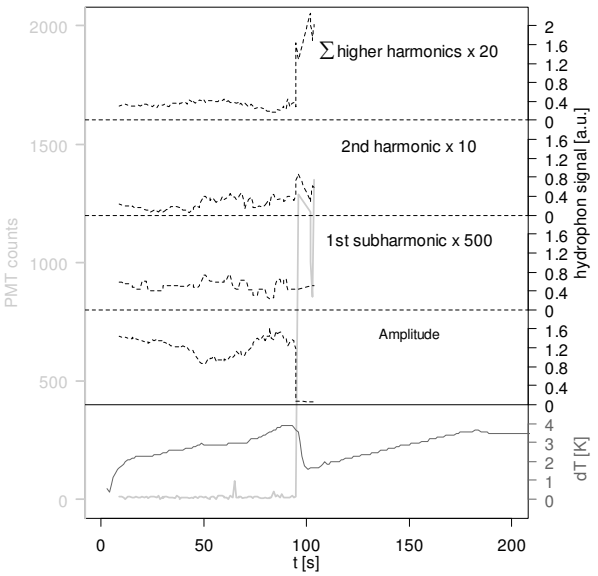

Figure 6 d. Photomultiplier signal, differential temperatur measurement and sound spectrum for Argon at 102% gasification and a power density of 3 W/cm^2.

In case of gasification levels at or exceeding saturation (Figures 6 c and d), the acoustic emission spectra show less clear response (neither do the *dT*-measurements). However, the overall acoustic activity seems to be slightly enhanced due to the presence of pre-nucleated bubbles at the very beginning of the sonication process. [32] An explanation could be the higher density of bubbles present in the sound field, which might lead to shielding effects and result in rather uncoherent

acoustic scattering at higher gasification level. [33] This explanation is supported by the difference in photon counts observed between gasification levels of 100 and 102%, once SL sets on. At this point, the emission is continous (though again preceeded by short burst of "premature" SL) and marked by a decrease in acoustic amplitude, a drop in temperature and an increase in the overall signal strength in the higher harmonic region. A self-supported process has therefore set on, where bubbles have reached a state of transient collapse and continously produce microbubbles that become immediately transient themselves. Characteristic for this state is enhanced acoustic scattering in a broad high-frequency band. As these higher frequencies are absorbed very efficiently, they will heat the liquid in the very vicinity of the transient bubbles, leading to significant heating of the liquid volume at sufficient bubble densities. This is shown in Figure 6 d: The sonoluminescent (and thus transient) regime sets on around 100 s after turning on the megasonic power. The temperature is intermediately dropping as the boundary layer heating is reduced due to the attenuation of the sound field. However, the bulk liquid is now heating up at a rate of 1K/min, reaching a temperature of around 4K above the initial temperature, when the sound field is deactivated after approximately 3 min.

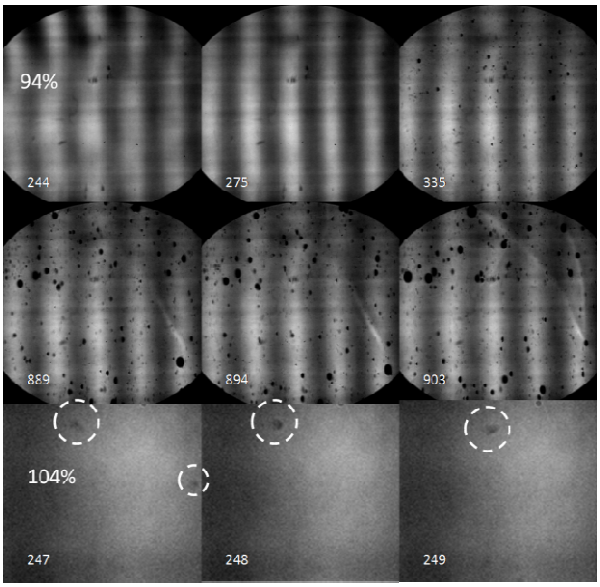

Figure 7. Sequence of stroboscopic Schlieren-images at 94 and 104% gasification respectively. The frames are numbered according to their appearance in the sequence. (framerate 500 1/s)

To investigate the transition to the transient regime, we employed a stroboscopic high-speed Schlieren-imaging technique [34] in order to visualize the interaction of the transient and nucleating bubbles with the sound field (Figure 7). Sequences shot at a framerate of 500 s^{-1} show the evaluation of the bubble nucleation process at 94% gasification level after 2.5 min of sonication. Initially, the acoustic field is distorted due to the presence of bubbles, which already have nucleated near the damping material and partially reflect the acoustic field. Prior to the onset of the transient state the acoustic field stabilizes due to increased acoustic scattering by the active bubbles in the bulk liquid. Presumably, the increased attenuation of the sound field reduces the portion, which is being reflected. (frames 244-335)

Subsequently bubbles start to nucleate and grow rapidly. In a later stage, this process is accompanied by convection streaming (frames 889-903) which is initiated by the presence of transient bubbles and their thermal activity. Such streaming is not found at higher gasification levels (likely due to the occuring screening effects in dense bubble populations). Instead, we were able to find micronsized pre-nucleated bubbles (frames 247-249) present in the supersaturated liquid, which promote and thus accelerate the onset of the transient state.

CONCLUSIONS

In the present work we show that a correlation of acoustic emission, acoustic heating and sonoluminescence detection can help to identify different regimes in the cavitation cycle. Without continous exchange of the liquid volume, the onset of the nucleation process is somewhat delayed. This is caused by the confined nucleation of bubbles at certain position in the sound field, where they are unable to spark the transient cavitation cycle. Instead, they locally alter the acoustic properties of the liquid and reduce the effective pressure amplitude. They cannot become transient, but remain acoustically and thermally active until they have grown out of their respective resonance. At saturation and above, micronsized bubble nuclei are already present in the liquid, so that the transient stage is reached very fast. It is characterized by continous emission of sonoluminescence, heating of the liquid volume and –at low gasification levels and thus reduced bubble-bubble interaction- the onset of convection streaming. The bubble grow rates in this stage are much faster than predicted. This leads to the assumption that the rectified diffusion promoted is accelerated by the heating due to the reduced solubility of gases at higher water temperature.

ACKNOWLEDGEMENTS

We would like to thank Philip de Greef (KU Leuven), Albert Debie and Geert Doumen (IMEC) for their technical support.

REFERENCES

1 C.D. Ohl, M. Arora, R. Dijkink, V. Janve and D. Lohse, "Surface cleaning from laser-induced cavitation bubbles", Appl. Phys. Lett. 89, p. 074102 (2006)
2 W. Kim, T.-H. Kim, J. Choi, and H.-Y. Kim, "Mechanism of particle removal by megasonic waves", *Appl. Phys. Lett.* **94**, p. 081908 (2009)
3 G. Vereecke, F. Holsteyns, S. Arnauts, S. Beckx, P. Jaenen, K. Kenis, M Lismont, M. Lux, R.Vos, J. Snow and P.W. Mertens, "Evaluation of Megasonic cleaning for sub-90 nm technologies", *Solid State Phenomena* **103**, p.141 (2005)
4 T.G. Leighton, "The forced bubble" in *The Acoustic Bubble* (Academic Press, London 1994)
5 L.A. Crum, G.M. Hnasen, "Growth of air bubbles in tissue by rectified diffusion", *Phys. Med. Biol.* **27**, p. 413 (1982)
6 R. Esche, "Untersuchung der Schwingungskavitation in Flüssigkeiten", *Acoustica* **2**, p. AB208 (1952)
7 J. Wu, "Temperature Rise generated by ultrasound in the presence of contrast agent", *Ultrasound Med. Biol.* **24**, p. 267 (1998)
8 S. Hilgenfeldt, D. Lohse, M. Zomack, *J. Acoust. Soc. Am.* **107,** p. 3530 (2000)
9 W.B. McNamara III, Y.T. Didenko and K.S. Suslick, "Sonoluminescence temperatures during multi-bubble cavitation", *Nature* **401**, p. 772 (1999)
10 E. Gonze Y. Gonthier, P. Boldo and A. Bernis, "Standing Waves in a high frequency sonoreactor: Visualization and Effects", *Chem. Eng. Sci.* **53**, p. 523 (1998)
11 L. Wang, H. Mitome, T. Kozuka, T. Tuziuti, "Influence of the Sound Field on the Intensity of Sonoluminescence", *Jpn. J. Appl. Phys*. **37,** p. 2832 (1998)

12 A.I. Eller and H.G. Flynn , "Rectified Diffusion through nonlinear pulsations of cavitation bubbles", *J. Acoust. Soc. Am* . **37**, p. 493 (1965)
13 C.C. Church , "Prediction of rectified diffusion during nonlinear bubble pulsations at biomedical frequencies", *J. Acoust. Soc. Am* . **83**, p. 2210 (1988)
14 J.B. Keller and M. Miksis, "Bubble Oscillations of large Amplitude", *J. Acoust. Soc. Am* . **68**, p. 628 (1980)
15 A. Prosperetti, "Thermal effects and damping mechanisms in the forced radial oscillations of gas bubbles in liquids", *J. Acoust. Soc. Am* . **61**, p. 17 (1977)
16 D. Lohse and S. Hilgenfeldt , "Inert gas accumulation in sonoluminescenscing bubbles", *J. Chem. Phys.* **107**, p. 6986 (1997)
17 W. Lauterborn , "Numerical investigation of nonlinear oscillations of gas bubbles in liquids", *J. Acoust. Soc. Am* . **59**, p. 283 (1976)
18 P.M. Morse and K.U. Ingard, "The radiation of Sound" in *Theoretical Acoustics* (McGraw-Hill, New York 1968)
19 S. Hilgenfeldt, D. Lohse and M. Zomack, "Sound scattering and localized heat deposition of pulse-driven microbubbles", *J. Acoust. Soc. Am* . **107**, p. 3530 (2000)
20 V. Kamath and A. Prosperetti, "Numerical integretaion methods in gas bubble dynamics", *J. Acoust. Soc. Am* . **85**, p. 1538 (1989)
21 B.E. Noltingk and E.A. Neppiras, "Cavitation produced by ultrasonics", *Proc. Phys. Soc. London Sect.* B**63**, p. 674 (1950)
22 A.I. Eller and H.G. Flynn , "Generation of subharmonics of order one-half by bubbles in a sound field", *J. Acoust. Soc. Am* . **46**, p. 722 (1969)
23 E.A. Neppiras and E.E. Fill, "A cyclic cavitation process", *J. Acoust. Soc. Am* . **46**, p. 1264 (1969)
24 E.A. Neppiras, "Acoustic Cavitation", *Phys. Rep.* **61**, p. 159 (1980)
25 P.M. Morse and K.U. Ingard, "Acoustic Wave Motion" in *Theoretical Acoustics* (McGraw-Hill, New York 1968)
26 G. K. Batchelor, "The physical properties of fluids" in *An introduction to fluid dynamics* (Cambridge University Press, 1967)
27 J.Wu, "Temperature rise generated by ultrasound in the presence of contrast agent", *Ultrasound in Med. & Biol.* **24**, p. 267 (1998)
28 S. Hilgenfeldt and D. Lohse, "The acoustics of diagnostic microbubbles: dissipative effects and heat deposition", *Ultrasonics* **38**, p. 99 (2000)
29 D. Razansky, P.D. Einziger and D.R. Adam, **"**Enhanced Heat Deposition Using Ultrasound Contrast Agent - Modeling and Experimental Observations", *IEEE Trans.Ultrason., Ferroelect., Freq. Contr.* **53**, p. 137 (2006)
30 F. Holsteyns, A. Riskin, G. Vereecke, A. Maes and P.W. Mertens, "Evaluation of megasonic cleaning process", *ECS Proc.* **26**, p. 161 (2003)
31 Y.T. Didenko and S.P. Pugach, "Spectra of Water Sonoluminescence", *J. Phys. Chem.* **98**, p. 9742 (1994)
32 M. Hauptmann, S. Brems, E. Camerotto, A. Zijlstra, G. Doumen, T. Bearda, P.W. Mertens and W. Lauriks, "Influence of gasification on the performance of a 1 MHz nozzle system in megasonic claening", *Microelectronic Engineering **87***, p. 1512 (2010)
33 N. Segebarth, O. Eulaerts, J. Reisse, L.A. Crum and T.J. Matula, "Correlation between Acoustic Cavitation Noise, Bubble Population, and Sonochemistry", *J. Phys. Chem. B* **106**, p.9181 (2002)